Available online at www.sciencedirect.com
SCIENCE DIRECT
Intermetallics 14 (2006) 54–60
Intermetallics
www.elsevier.com/locate/intermet

Neutron diffraction study of oxygen dissolution in α_2-Ti_3Al

Camille Y. Jones[a,*], William E. Luecke[b], Evan Copland[c]

[a]NIST Center for Neutron Research, National Institute of Standards and Technology, Gaithersburg, MD 20899, USA
[b]Metallurgy Division, National Institute of Standards and Technology, Gaithersburg, MD 20899, USA
[c]Case Western Reserve University and Materials Division, NASA Glenn Research Center, Cleveland, OH 44135, USA

Received 30 March 2004; accepted 12 April 2005
Available online 27 June 2005

Abstract

Rietveld refinements of neutron powder diffraction data on α_2-Ti_3Al have been performed to determine the crystal structure as a function of interstitial oxygen (O) concentration for three alloys with a Ti/Al ratio of $\approx$2.34 and O concentrations of 0.25, 3.99, and 7.71%. The structures of the alloys are hexagonal in space group *P6$_3$/mmc* where Ti and Al atoms populate unique sites with excess Al at the Ti site and O atoms occupy octahedral interstitial sites surrounded by six Ti sites. The length of the *c*-axis was found to increase linearly as the O occupancy of the interstitial sites increased; this lattice lengthening effect was much less pronounced along the *a*-axis. Correspondingly, the increases in the lengths of Ti–Al and Ti–Ti bonds with a major component of their direction parallel to the *c*-axis were roughly an order of magnitude greater than the increases in the lengths of Ti–Al and Ti–Ti bonds more closely aligned with the *a*-axis. Densities calculated from the lattice parameters and occupancy factors fall in the range (4.118 ± 0.004) to (4.194 ± 0.004) g/cm^3, and exhibit a nearly linear increase with oxygen concentration. Measured densities of (4.113 ± 0.001), (4.146 ± 0.009), and (4.191 ± 0.002) g/cm^3 for these alloys agree with the results of the refinements.
Published by Elsevier Ltd.

Keywords: Titanium aluminides based on Ti_3Al (A); Neutron diffraction (F); Site occupancy (E); Crystal chemistry (B); Interstitial oxygen

1. Introduction

Interstitial species are an important issue for titanium-rich alloys, particularly those in the Ti–Al system. The high solubility of interstitials such as oxygen has a strong influence on high-temperature phase equilibria. The wide range of phase equilibria initially reported (1951–1987) for the Ti-rich side of the Ti–Al system has been attributed to inadequate knowledge of the concentration of interstitials as well as an inability to differentiate between disordered *hcp* α-Ti and ordered α_2-Ti_3Al [1,2]. With the distinction between α-Ti and α_2-Ti_3Al now being understood, investigation of its phase equilibria with β-Ti, α-Ti and γ-TiAl above 1100 °C continues with the development of γ-TiAl based intermetallic alloys for high temperature structural applications [3]. The alloys of interest typically contain both γ-TiAl and α_2-Ti_3Al and are based on a composition with 48 atom % aluminum (Ti–48%Al). The phase γ-TiAl has an ordered $L1_0$ face-centered tetragonal structure in space group *P4/mmm* with a composition range 49–60% Al and excess Al substituted randomly at Ti sites. The phase α_2-Ti_3Al has composition range 22.5% to 39% Al with an ordered DO_{19}-type structure (space group *P6$_3$/mmc*) where the Ti atoms are slightly displaced from the ideal positions of a regular *hcp* structure, suggesting a strong tendency toward covalent bonding between Ti and Al [4]. In α_2-Ti_3Al, excess Al also substitutes randomly at the Ti lattice site.

The high solubility of interstitials such as oxygen also has a detrimental effect on mechanical properties of alloys in the Ti–Al system. A major limitation to the application of γ-TiAl-based alloys is their poor oxidation resistance, characterized by the formation of a non-protective, mixed $TiO_2 + Al_2O_3$ scale [5]. For good oxidation resistance above 900 °C, the formation of a protective α-Al_2O_3 layer is required. However, the high solubility of oxygen in α_2-Ti_3Al inhibits the formation of α-Al_2O_3. Experimentally determined Ti–Al –O phase diagrams indicate α_2-Ti_3Al + γ-TiAl mixtures occur only when in equilibrium with α-Al_2O_3, but this three-phase mixture only occurs under

* Tel.: +310 975 4507; fax: +301 921 9847.
E-mail address: camille.jones@nist.gov (C.Y. Jones).

0966-9795/$ - see front matter Published by Elsevier Ltd.
doi:10.1016/j.intermet.2005.04.011

conditions of oxygen saturation [6–8]. The major component of the γ-TiAl-based alloy microstructure is γ-TiAl (80–90% by volume), which has limited oxygen solubility, (0.025 ± 0.05)% O, compared to α_2-Ti_3Al (10–15% O). Such a high oxygen content is unacceptable to the preservation of the desirable mechanical properties of these alloys.

The dramatic difference in oxygen solubility between γ-TiAl and α_2-Ti_3Al identifies α_2-Ti_3Al as an important factor in the achievement of a better understanding of α-Al_2O_3 scale formation. It is thus surprising that only limited data are available to explain the high solubility of oxygen in α_2-Ti_3Al. The only discussion found in the literature is a study by Menand et al. [9] which proposed that the large difference in oxygen solubility was due to the different types of octahedral sites present in α_2-Ti_3Al and γ-TiAl. Similar to the octahedral environments identified for interstitial carbon and nitrogen in Ti by Jeitschko et al. [10] the octahedral sites surrounded by six Ti atoms [OTi_6] in α_2-Ti_3Al may explain the higher solubility of oxygen. Further study and understanding of oxygen solubility in α_2-Ti_3Al are needed to facilitate the discovery of conditions which promote the formation of protective α-Al_2O_3 scale.

The current investigation studied the effect of dissolved oxygen on the structure of α_2-Ti_3Al for an approximately constant titanium-to-aluminum (Ti/Al) ratio. High-resolution neutron powder diffraction and Rietveld refinement were employed to provide direct evidence for the site occupancy of dissolved oxygen and to study its effect on the crystal structure. Bulk density measurements were performed to confirm the structure refinements. Results are presented for oxygen site occupancy and structural changes with oxygen concentration. Neutron diffraction was the ideal method for this investigation, due to the depth of penetration of neutrons, high contrast afforded by the negative scattering length of Ti, and comparable sensitivity of the technique to all Ti, Al, and O.

2. Experimental

2.1. Alloy preparation

The ternary α_2-Ti_3Al(O) alloys (≈100 g) were produced by arc melting the appropriate portions of pure-Ti (99.995% by weight), pure-Al (99.995% by weight) and pure TiO_2 (99.99% by weight) under an oxygen-gettered, high purity Ar atmosphere and drop casting into a chilled Cu mold. To ensure an equilibrium structure, each alloy was homogenized at 1100 °C for 200 h and water quenched. During annealing, an inert atmosphere was provided by wrapping each sample in a tantalum-foil envelope and vacuum encapsulating in a quartz ampoule. The compositions of the alloys were measured multiple times by a combination of inductively coupled plasma atomic absorption spectroscopy, gas fusion, and wet chemistry and average values are listed in Table 1. The Ti/Al ratio of the three samples was 2.30–2.37. The high oxygen concentrations of alloys number 5 (A5) and number 8 (A8) allowed them to be crushed and divided into two groups with particle sizes greater than and less than 150 μm. Alloy 2 (A2) was too ductile to be crushed, so a single solid, cylindrical piece was used for the measurements described below.

Table 1
Measured composition of α_2-Ti_3Al(O) alloys. The relative uncertainties in the compositions are approximately 1%

Alloy	Elemental composition (%)	Ti/Al
2	Ti-70.17, Al-29.56, O–0.25	2.37
5	Ti-67.37, Al-28.49, O–3.99	2.37
8	Ti-64.26, Al-27.99, O–7.71	2.30

2.2. Neutron diffraction measurements

Data were collected using the BT-1 32-detector neutron powder diffractometer at the NIST Center for Neutron Research. The instrument settings were a Si(531) monochromator with a wavelength of 1.590 Å, a take-off angle of 120 °, and in-pile collimation of 15 min of arc. The beam was masked to 1.59 cm × 5.08 cm at the sample. Measurements were made on 20 g of cast and ground alloys in a vanadium-can, 5.08 cm long and with a 1.56 cm O.D. Data were collected over the range of $3\,^\circ < 2\theta < 165\,^\circ$ with a step size of 0.05 ° 2θ. Preliminary scans revealed strain broadening in samples ground to particle sizes of <150 μm, therefore samples with particle sizes of >150 μm were measured.

2.3. Density measurements

The densities were measured using Archimedes' method (Table 2). A2 was a cylindrical specimen ~3 cm long and 1 cm in diameter while A5 and A8 were smooth but irregularly shaped specimens. The specimens were weighed in both air and distilled water that was in thermal equilibrium with the laboratory, typically about (22 ± 0.1) °C. The specimens were submerged in the distilled water for several hours to ensure all bubbles adhering to the specimen had dissolved and this was visually verified before weighing. Calibrated density floats made of borosilicate glass filled with lead shot (R.P. Cargille Laboratories, Cedar Grove, NJ) [11] and certified to an accuracy of 0.0005 g

Table 2
Densities determined by Archimedes' method

Alloy	Weight of specimen (g)	Average density (g/cm^3)[a]	Number of measurements
2	11.2369	4.113(1)	3
5	1.2357	4.146(8)	5
5	2.0525	4.145(3)	5
8	15.1801	4.191(2)	5

[a] Standard uncertainty in parentheses in g/cm^3.

Table 3
Initial structure model in space group $P6_3/mmc$

a/(nm)	*c*/(nm)	*Atom*	*X*	*y*	*Z*	*f*	*Wyckoff symbol*	*Symmetry*	*Multiplicity*
0.5792	0.4648	Ti	5/6	2/3	1/4	1	*H*	*mm2*	6
		Al	1/3	2/3	1/4	1	*C*		2
		O	0	0	0	*N*[a]	*A*		2

[a] *n* Is the occupancy of the O site; $n=0.0$ for A2, 0.179 for A5, and 0.373 for A8.

cm^{-3} were also measured for comparison with the alloy results.

3. Structure refinement

The initial structure model is listed in Table 3. The lattice parameters are those reported by Goldak and Parr [12], and the initial structure parameters for α_2-Ti_3Al are from Gehlen [4], with the Ti and Al atoms placed at their ideal positions in the Ti_3Sn-type structure. The O site was placed at the origin of the unit cell, surrounded by six Ti sites in an octahedral arrangement. The initial occupancy factors for Ti and Al (f_{Ti} and f_{Al}) were unity; the initial occupancy factor for O was either set at zero or at values calculated from the measured concentrations for each alloy. Refinement of the structures was performed with the General Structure Analysis System (GSAS) [13] suite of programs with the EXPGUI graphical user interface to GSAS [14]. Neutron scattering lengths, provided in GSAS, are those from the tabulation of Sears [15]. The bound coherent scattering lengths for Ti, Al, and O are (-343.8 ± 0.2) fm^2, (344.9 ± 0.5) fm^2, and (667.1 ± 0.4) fm^2, respectively. The diffraction patterns for all three alloys indicated single-phase materials with no additional reflections from impurities. The widths of the reflections were at the limit of instrument resolution across the entire angular range. Single-phase refinements were performed on total intensity vs. 2θ with scale factor and background (a 10-term Chebyshev polynomial), lattice parameters, diffractometer zero, peak profiles (Gaussian modified for peak asymmetry), atom positions, fractional occupancy, and parameters for isotropic atomic displacement, U_{iso}. In the initial stages of the refinement, satisfactory fits to scale factor, background, lattice parameters, diffractometer zero, and peak profiles were obtained from a LeBail fit [16] to the reflection intensities, i.e. by iterations of the Rietveld decomposition to fit the observed intensities without a structure model. Later stages of the structure refinement involved Rietveld refinement of structure and atomic displacement parameters. Given the total masses and number densities of Ti, Al, and O in the samples, the absorption cross sections for the elements were sufficiently low that an absorption correction was not necessary. Fractional occupancies for both Ti and Al were refined at each metal site. Parameters were refined to convergence, i.e., until the shifts in the parameters were 1% of the estimated standard deviation.

4. Results

4.1. Lattice parameters

Refined lattice parameters and calculated volumes and densities for the three alloys are tabulated in Table 4. The lattice parameter *a* for A2 is consistent with the value of Clark *et al*. [17] As shown in Fig. 1, the lattice parameters increase approximately linearly with increasing O content, the expansion along *c* being one order of magnitude larger than that in the basal plane. Least-squares fits of *a* and *c* with second-order polynomials yielded the expressions

$$a/nm = -0.000006x_0^2 + 0.00012x_0 + 0.57818 \quad (1)$$

$$c/nm = 0.00001x_0^2 + 0.00036x_0 + 0.46395 \quad (2)$$

where x_0 is percent oxygen. The R^2 values for the fits were both unity. The degree of lattice expansion with dissolved oxygen observed for α_2-Ti_3Al in this study, expressed as

Table 4
Refined lattice parameters and calculated volumes and densities

Alloy	a (nm)	c (nm)	Volume of unit cell (nm)^3	Density (g/cm^3)
A2	0.578167(4)	0.463949(5)	0.13431	4.118(4)
A5	0.578543(4)	0.465629(6)	0.13497	4.153(4)
A8	0.578702(6)	0.467783(7)	0.13567	4.194(4)

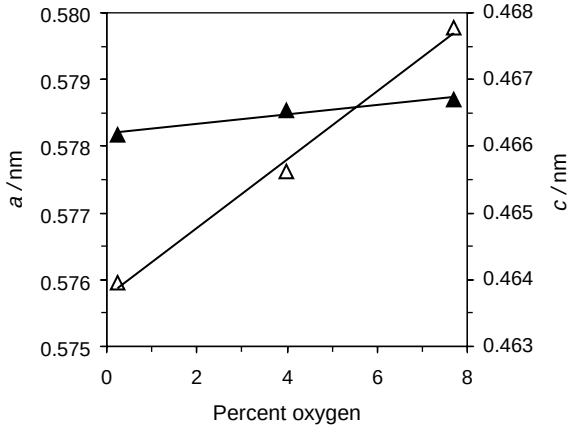

Fig. 1. Lattice parameters versus percent oxygen for A2, A5, and A8. The error bars are smaller than the symbols. Open triangle correspond to the *c*-axis.

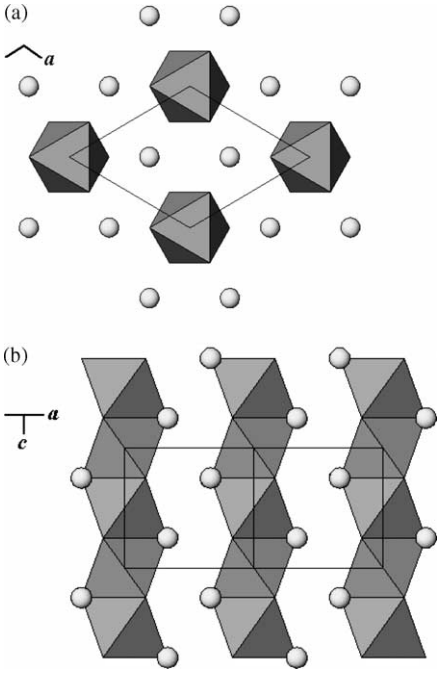

Fig. 2. Crystal structure of α_2-Ti_3Al(O) viewed along two directions: a, [001]; b, [110]. The spheres represent Al atoms and the octahedra represent [OM_6] groups (M = Ti or Al).

$da/dx_o = 0.00012$ nm/%O and $dc/dx_o = 0.00036$ nm/%O, agree with those reported for dilute hcp α-Ti, 0.00016 nm/%O and 0.00063 nm/%O, respectively [18]. This degree of expansion is consistent with oxygen taking the [OTi_6] octahedral sites. The densities calculated from the lattice parameters and occupancy factors fall in the range (4.118 ± 0.004)–(4.194 ± 0.004) g/cm^3, and thus also exhibit a roughly linear increase with increasing oxygen content.

4.2. Crystal structures

The structures of the alloys are hexagonal in space group *P6$_3$/mmc*. The crystal structure, drawn in Fig. 2, is similar to that of the previously determined α_2-Ti_3Al intermetallic phase with the addition of O atoms at octahedral interstices surrounded by six Ti atom sites. The [OTi_6] octahedra are face-sharing and form rows along *c*. The Ti and Al atoms are ordered on two crystallographically unique sites, with excess Al at the Ti site. Refined structure parameters and refinement statistics are listed in Tables 5 and 6. In all cases, the occupancy of the Al site refined to unity within the uncertainty of the measurement. For A5 and A8, similar results were obtained for the occupancies of Ti and Al on the Ti site, whether refined from a value of either $f_{Ti} = 1$ or from the calculated site occupancies listed in Table 3. The occupancy factors yielded values close to the measured compositions. A representative refinement is shown in Fig. 3.

The lattice expansion with increasing O content corresponds to increases in the Ti–Ti and Ti–Al bond distances. Selected bond distances for the three alloys are listed in Table 7. The nearest-neighbor coordinations around Ti and Al are shown in Figs. 4 and 5. The most pronounced changes are in the Ti–Al bonds roughly along *c*, which increase from (0.2839 ± 0.0003) nm in A2 to (0.2857 ± 0.0003) nm in A8, and the Ti–Ti bonds along *c*, from (0.2877 ± 0.0003) nm in A2 to (0.2892 ± 0.0003) nm in A8. The increases in length are roughly linear for the Ti–Al and Ti–Ti distances, approximately 0.002 and 0.0024 nm, respectively, for every 1% increase in O. The Ti–Al contacts in the basal plane increase in length with increasing O content, but the effect is one order of magnitude smaller than in the direction of *c*. The longest distances overall are the Ti–Ti contacts on the shared faces of octahedra in the basal plane.

4.3. Bulk densities

Table 2 lists the density results for the alloys. A comparison of the measured and calculated densities shows the two results to be identical within the estimated uncertainties and indicates fully dense materials. The value for A2 is slightly less than 4.12 g/cm^3, the density determined for as-cast α_2-$Ti_{69.5}Al_{30.5}$ [19]. For the alloy specimens, whose weights were on the order of several grams, the largest contribution to the uncertainty in measured density was the difficulty in measuring the specimen weight in the liquid. The correction for thermal

Table 5
Structural parameters

Alloy	Atom	*x*	*y*	*Z*	*f*	$U_{iso}/(10^2$ nm$^2)$
A2	Ti	0.8301(1)	0.6602(3)	1/4	0.929(2)	0.0109(3)
	Al	0.8301(1)	0.6602(3)	1/4	0.071(2)	0.0109(3)
	Al	1/3	2/3	1/4	1	0.0109(3)
	O	0	0	0	0.024(2)	0.0054(6)
A5	Ti	0.83053(8)	0.6611(2)	1/4	0.927(2)	0.0100(2)
	Al	0.83053(8)	0.6611(2)	1/4	0.073(2)	0.0100(2)
	Al	1/3	2/3	1/4	1	0.0095(2)
	O	0	0	0	0.173(2)	0.0078(5)
A8	Ti	0.8303(1)	0.6606(2)	1/4	0.920(2)	0.0096(2)
	Al	0.8303(1)	0.6606(2)	1/4	0.080(2)	0.0084(2)
	Al	1/3	2/3	1/4	1	0.0096(2)
	O	0	0	0	0.359(3)	0.0067(5)

Table 6
Refinement statistics

Alloy	Number of data	wR_F [a]	χ_r^2
A2	3202	0.0811	2.01
A5	3207	0.0513	1.41
A8	3099	0.0669	1.54

[a] wR_F is the weighted R factor calculated on the structure factor, F.

expansion and thus the density of water is given by the equation

$$\rho(T) = 1.0007 - 0.89639 \times 10^4 T - 0.18593 \times 10^{-6} T^2 - 0.84409 \times 10^{-7} T^3 \quad (3)$$

where T is in degrees Celsius. The correction for the water density changes the apparent density of the specimen by an amount equivalent to a temperature change of 0.0008 °C; this correction is small compared to the other uncertainties. The densities of the specimens were not corrected back to standard conditions; however, such a correction would be much less than the uncertainty of the technique.

5. Discussion

This study has provided clear evidence that oxygen dissolves interstitially in α_2-Ti_3Al at octahedral sites surrounded by six Ti atom sites as was previously suggested [9,10,18]. The oxygen dissolution can be considered primarily as an interaction between oxygen and the Ti sublattice, independent of the Al in α_2-Ti_3Al. However, the presence of Al at the Ti site in α_2-Ti_3Al reduces the number of [OTi_6] sites available to accept dissolved oxygen. This behavior corresponds to that observed in the binary systems, where the Ti–O system exhibits wide solubility ranges and the formation of a large number of crystalline-phases, while in the Al–O system only α-Al_2O_3 is formed.

This study has also shown the distortions that occur in the structure of α_2-Ti_3Al with increasing O content for a constant Ti/Al ratio. As the occupancy of O at [OTi_6] interstitial sites increases, the Ti–Al and Ti–Ti bonds with the major component of their direction parallel to c become longer. The corresponding change in the same bond lengths in the direction of a is an order of magnitude smaller than in the direction of c. The elongation of the metal-metal bonds indicates a weakening of the bonding with increasing O content.

At the concentration of Ti used for the present study, corresponding to a Ti/Al ratio of 2.37, and assuming that all [OTi_6] sites are filled, the maximum O solubility in the α_2-Ti_3Al structure is about 14%. However, the maximum O content observed experimentally [8] in α_2-Ti_3Al at this Ti/Al ratio is closer to 10%, or 2/3 occupancy of the octahedral sites. Above this concentration, a two-phase mixture of α_2-Ti_3Al(O) and α_2-Al_2O_3 is formed. The solubility limit for O in α_2-Ti_3Al thus falls considerably below the level predicted from the number of interstitial sites available to O, but above the 50% occupancy corresponding to the maximum gain in configurational entropy. This suggests a degree of ordering of oxygen on the [OTi_6] sites due to an interaction

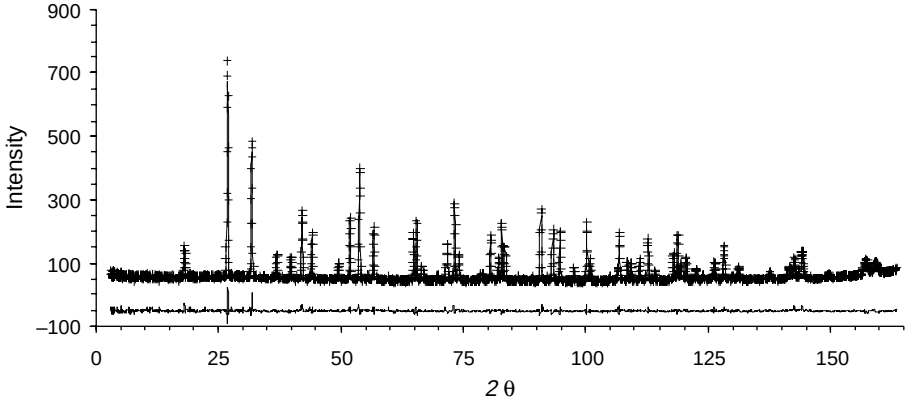

Fig. 3. Refinement results for α_2-Ti_3Al(3.99%O): crosses: observed intensities; solid line: calculated intensities; lower solid line: residuals.

Table 7
Ti–Ti and Ti–Al nearest-neighbor distances

Ti–Al distance (nm)			Ti–Ti distance (nm)		
O content/ percent	Along c	In basal plane	Between octahedra	Within octahedra in basal plane	Within octahedral along c
0.25	0.2839	0.2891	0.2835	0.2947	0.2877
3.99	0.2849	0.2893	0.2844	0.2941	0.2882
7.71	0.2857	0.2894	0.2841	0.2946	0.2892

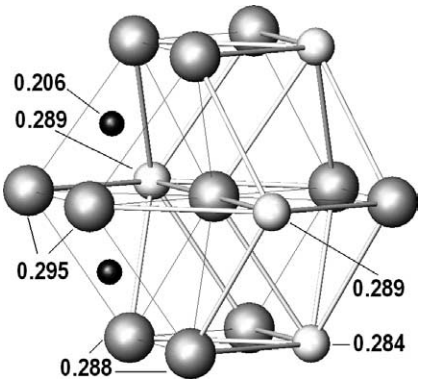

Fig. 4. Coordination around Ti (center sphere) for A2. The distances from the center Ti atom to the marked Ti (large dark grey), Al (small light grey), and O (black) atom sites are given in nanometers.

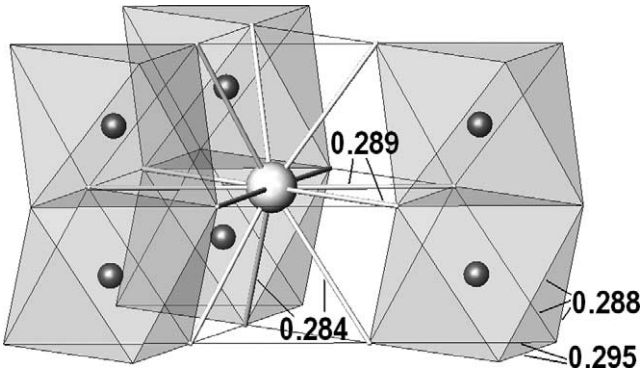

Fig. 5. Coordination around Al (center, light grey sphere) for A2. Ti–Al bonds in the basal plane are 0.289 nm, and Ti–Al bonds with their major component along *c* are 0.284 nm. Ti–Ti bonds in the basal plane are 0.295 nm, and Ti–Ti bonds with their major component along *c* are 0.288 nm. Oxygen sites are indicated by black spheres. Arrow points to the center Ti atom in figure.

between O atoms as their concentration increases. The likelihood of the occupation of a particular interstitial site by O may in fact depend on the fraction, or probability, of Ti (or Al) surrounding that site. For reasons of stability, O dissolution may force a nonrandom occupation of excess Al from an otherwise random occupation [20] of Al at Ti sites. Further insights on the effects of the dissolution of O or other interstitial species on the structure of α_2-Ti_3Al and its stability relative to α-Al_2O_3 would be gained from an investigation of the short-range order surrounding the O octahedral sites.

6. Summary and conclusions

Rietveld refinements of neutron powder diffraction data on α_2-Ti_3Al clearly show small but significant distortions in the structure of α_2-Ti_3Al as the concentration of interstitial oxygen increases. As O concentration at interstitial sites increases, the Ti–Al bonds with the major component of their direction parallel to *c* become longer, with the lengthening of bonds in the direction of *a* one order of magnitude smaller than in the direction of *c*. Overall, the shortest bonds are those in the basal plane between Ti atoms in neighboring octahedra, and the longest bonds overall are the Ti–Ti contacts on the shared faces of octahedra in the basal plane. Densities of the alloy also increase with increasing O content. An observed solubility limit of oxygen filling fewer than the total available interstitial sites suggests short-range ordering of the oxygen on the [OTi_6] sites and ordering of excess Al on the Ti sublattice. The bond distances extrapolated to the observed solubility limit may be important structural indicators of the stabilization of α-Al_2O_3 relative to α_2-$Ti_3Al(O)$. These results highlight the notion of structurally based limits to oxygen dissolution in α_2-Ti_3Al on the stabilization of α-Al_2O_3 and the need for a better understanding the structural effects of interstitials for the continued development of γ-TiAl based intermetallic alloys.

Acknowledgements

The authors are grateful for funding from the High Operating Temperature Propulsion Components and Ultra-Efficient Engine Technology Projects at Glenn Research Center, Cleveland, OH.

References

[1] Mishurda JC, Perepezko JH. Microstructure/property relationships in titanium aluminide alloys. In: Kim Y-W, Boyer RR, editors.. TMS; 1991. p. 3–30.
[2] Flower HM, Christodoulou J. Mater Sci Tech 1999;15:45–52.
[3] Ohuma I, Fujita Y, Mitsui H, Ishikawa K, Kainuma R, Ishida K. Acta Mater 2000;48:3113.
[4] Gehlen PC. In: Jaffee RI, Promisel N, editors. The science technology and application of titanium. Oxford: Pergamon Press; 1970. p. 349–57.
[5] Rahmel A, Quadakkers W, Schütze M. Mater Corrosion 1995;46:271.
[6] Li XL, Hellel R, Teyssandier F, Choi SK, van Loo FJJ. Acta Metall 1992;40:3149.
[7] Zhang M-X, Hsieh K-C, DeKock J, Chang YA. Scripta Metall 1992; 27:1361.
[8] Copland, E. PhD Thesis. Thermodynamics and kinetics of interfacial reactions in the Ti–Al–O system, School of Materials Science and Engineering, University of New South Wales, Sydney, Australia; 1999.
[9] Menand A, Huguet A, Nerac-Partaix A. Acta Mater 1996;44(12): 4729–37.
[10] Jeitschko W, Nowotny H, Benesovsky F. J Less-Common Metals 1964;7:133–8.
[11] Certain commercial materials are identified in this paper to foster understanding. Such identification does not imply recommendation or endorsement by the National Institute of Standards and Technology, nor does it imply that the materials identified are necessarily the best available for the purpose.
[12] Goldak AJ. Gordon Parr. J AIME 1961;221:639–40.

[13] Larson AC, Von Dreele RB. General structure analysis system. LAUR 86-748.: Los Alamos National Laboratory; 1986.
[14] Toby BH. 'EXPGUI, a graphical user interface for GSAS.'. J Appl Cryst 2001;34:210–3.
[15] Sears VF. Neutron News 1992;3(3):26–37.
[16] LeBail A, Duroy H, Fourquet JL. Mat Res Bull 1988;23:447–52.
[17] Clark D, Jepson KS, Lewis GIJ. Inst Metals 1962-1963;91:197–203.
[18] Dechamps M, Quivy A, Baur C, Lehr P. Scripta Metallurgica 1977; 11:941–5.
[19] Braun J, Ellner MZ. Z Metallkd 2000;91:389–92.
[20] Lefebvre W, Loiseau A, Thomas M, Menand A. Phil Mag A 2002;82: 2341–55.